



This is a repository copy of *The phase-switched screen* .

White Rose Research Online URL for this paper:  
<http://eprints.whiterose.ac.uk/800/>

---

**Article:**

Chambers, B. and Tennant, A. (2004) The phase-switched screen. IEEE Antennas and Propagation Magazine, 46 (6). pp. 23-37. ISSN 1045-9243

<https://doi.org/10.1109/MAP.2004.1396733>

---

**Reuse**

Unless indicated otherwise, fulltext items are protected by copyright with all rights reserved. The copyright exception in section 29 of the Copyright, Designs and Patents Act 1988 allows the making of a single copy solely for the purpose of non-commercial research or private study within the limits of fair dealing. The publisher or other rights-holder may allow further reproduction and re-use of this version - refer to the White Rose Research Online record for this item. Where records identify the publisher as the copyright holder, users can verify any specific terms of use on the publisher's website.

**Takedown**

If you consider content in White Rose Research Online to be in breach of UK law, please notify us by emailing [eprints@whiterose.ac.uk](mailto:eprints@whiterose.ac.uk) including the URL of the record and the reason for the withdrawal request.



[eprints@whiterose.ac.uk](mailto:eprints@whiterose.ac.uk)  
<https://eprints.whiterose.ac.uk/>

# The Phase-Switched Screen

*Barry Chambers and Alan Tennant*

Department of Electronic and Electrical Engineering  
University of Sheffield

Mappin Street, Sheffield, S1 3JD, UK

Phone: +44 114 222 5588; +44 114 222 5438; Fax: +44 114 222 5834;

E-mail: b.chambers@sheffield.ac.uk; a.tennant@sheffield.ac.uk

---

## Abstract

Conventional (passive) radar-absorbent materials operate either by phase cancellation or by absorbing incident electromagnetic energy and converting it into heat. This paper examines a new type of active "absorber," called the phase-switched screen (PSS). The PSS operates quite differently from passive absorbers in that it exhibits an apparently low value of reflectivity by redistributing the electromagnetic energy incident upon it over a bandwidth that is wide enough to ensure that little reflected energy falls within the pass-band of the receiver. The discussion considers the basic temporal and spectral properties of several PSS topologies, and includes measured data on both planar and cylindrical PSS structures.

Keywords: Electromagnetic scattering; modulation; radar cross-sections; electromagnetic scattering by absorbing media; intelligent materials; intelligent structures

## 1. Introduction

Throughout history, humans have made use of stealth and deception, firstly as hunters and then as warriors. In modern warfare, these skills have become ever more important due to the widespread use of all-weather, long-range sensors such as radar. Even from the earliest days of large-scale deployment of operational radar systems, such as the UK Chain-Home system in the late 1930s, effort has been put into ways of negating the radar detection and tracking of a target. At that time, the importance of target shaping was not appreciated, and so attention was concentrated on the possible use of radar-absorbent materials (RAM) to reduce a target's radar cross section (RCS). The earliest known RAM was that developed in 1936 in the Netherlands, for use on antennas [1], but by the early 1940s, the basic principles of both resonant and lossy-layer RAM were widely known [2]. By 1945, these had been developed into the well-known Salisbury screen [3], and the Jaumann and Dallenbach absorbers [4]. For nearly 60 years, many RAM designs have remained basically the same as they were in the late 1940s. However, improvements in performance have been achieved through the incorporation of new materials such as ferrites, structural absorbers, and frequency-selective surfaces, and the wide spread use of computer-aided design [5-7]. The latter is crucial for the realization of a low-RCS vehicle, since, in practice, RAM treatments need to form an integral part of the vehicle design, so that non-specular wave propagation and scattering phenomena can be taken fully into account. Although in practice most RAM treatments are not in the physical form of flat panels, these are widely used in the research and development of new types of RAM, since this simplifies initial modeling and free-space testing. Hence, much of the discussion in this paper will be devoted to flat-panel RAM geometries.

So far, we have only considered what might be termed conventional or passive RAM. Although widely used, it does have

some disadvantages in practice. For example, RAM is designed to meet a particular specification with respect to frequency, bandwidth, and reflectivity level, etc. However, this specification is fixed at the time of manufacture, and so if during the lifetime of a RAM-covered platform the threat changes, then either the RAM has to be replaced, or a degraded performance against the new threat accepted. Also, as a number of authors have shown, the laws of physics limit the overall performance of passive RAM with regard to the reflectivity that can be achieved over a given band of frequencies for a given angle of incidence and polarization. Of particular interest is the lowest frequency at which a desired value of reflectivity can be achieved for a given electrical thickness of RAM [8]. One possible way of improving RAM might be to make it active, i.e., to incorporate some means of changing the electrical parameters of its constituent materials. This might be done by using volumetric change, through materials such as controllable conducting polymer composites [9] or photo-dielectrics [10], or by using discrete devices, such as semiconductor diodes [11-15]. Given that the same laws of physics will apply to both passive and active RAM, how can the latter improve on the former? Assume that in a particular electrical state, an active RAM has identical characteristics to its passive counterpart. If the electrical state of the active RAM is now changed, this will result in a new electromagnetic configuration, so its characteristics will also change and be different from those of the passive RAM. Hence, the active RAM may have superior characteristics to its passive counterpart, when measured in terms of the sum of its instantaneous bandwidths. This argument must be used with caution, however, as the active RAM cannot by this means be used to synthesize the ideal RAM, i.e., one having negligible reflectivity over all frequencies. To illustrate this, consider a simple active RAM structure, consisting of a Salisbury screen in which the normal resistive layer has been replaced by one incorporating a parallel arrangement of fixed resistance and controllable capacitance. The predicted static reflectivity characteristics for a range of capacitance values are

shown as dotted curves in Figure 1. Hence, provided that the RAM has to deal with only one threat frequency at a time, then it can indeed be tuned to have optimum performance over a wide band of frequencies. If, however, there are many simultaneous and widely spaced threat frequencies, then it is the time-averaged RAM reflectivity that is important. The solid curve in Figure 1 shows the resulting time-averaged reflectivity when there are six threat frequencies, equally spaced over a bandwidth of 5 GHz. Now the RAM performance is degraded, since it can only dwell on each threat frequency for one-sixth of the time (assuming equal dwell times); furthermore, the time-averaged reflectivity at a given frequency is also degraded by the skirts of the reflectivity characteristics when the RAM is tuned to the other frequencies. In summary, active RAM can only be effective provided that its conditions of use are carefully defined. When deployed correctly, however, active RAM may have additional functionality, such as being able to provide deception (e.g., instantaneous change from non-stealth to stealth mode, false Doppler), positive target identification (e.g., IFF: identification friend or foe), and smartness [16].

## 2. The Modulating Surface

The concept of a modulating surface was first discussed in the late 1940s [17], but then and in its recent practical implementations [18, 19] it was envisaged mainly as a means of covert communication. In this paper, however, we will discuss the application of a modulating surface to the problem of RCS control through its identity as an active "absorber." Unlike the RAM (active or passive) discussed in Section 1, this new class of "absorber" does not actually absorb the incident electromagnetic energy, but reflects it and at the same time redistributes it over a bandwidth that is so wide that little falls within the pass-band of the radar receiver. Therefore, in its broadest sense the reflected signal resembles that produced by a spread-spectrum transmitter. The simplest method of doing this would be to utilize the Doppler effect. Several authors have considered the periodic Doppler shift produced at microwave frequencies by a flat PEC plate that is vibrated with a sinusoidal displacement in a direction perpendicular to that of the incident wave vector [20, 21]. In this case, the incident energy is redistributed on reflection between a component at the incident carrier frequency,  $f_c$ , and an infinite number of sideband frequencies, which are determined by the plate vibration frequency,  $f_v$ , and the maximum velocity attained by the plate during its sinusoidal motion. Because not all the reflected energy is now at  $f_c$ , the vibrating surface appears to act as an "absorber" at this frequency, *as measured by the receiver*. Because of the obvious similarity to the process of angle modulation, the vibrating plate might be referred to as an "angle-modulating surface." To assess its usefulness in practice, consider the ideal case when all of the incident energy at  $f_c$  is to be redistributed among the reflected sideband components, and all are to lie outside the pass-band,  $2B$ , of the receiver. Following [21], the amplitude of the signal reflected from the plate at  $f_c$  is proportional to  $J_0(2f_c v_{max}/f_v c)$ , where  $J_0$  is the Bessel function of the first kind of order zero, and  $c = 3 \times 10^8$  m/s. Then, since  $J_0(x) = 0$  when  $x = 2.405$ , and letting  $f_c = 10$  GHz and  $f_v = B = 5$  MHz, the required value of  $v_{max}$  is approximately  $1.8 \times 10^5$  m/s. This results in a maximum plate displacement of approximately  $\pm 5.7$  mm. Clearly, these requirements are impractical for a large-area mechanically actuated system, and so an alternative modulating structure must be sought.

One solution lies in requiring the plate to be positioned repetitively at one of only two positions in space, rather than at an infinite number. This may be synthesized electronically, thus eliminating limitations on performance due to the inertia and mass of the plate. Thus, the "phase-switched screen" (PSS) achieves an effect similar to the angle-modulating surface, but by applying binary phase-shift modulation to the incident signal. This has the advantage that the resulting reflected signal will have inherent cancellation of the component at  $f_c$  [22].

Several approaches may be used to explore the properties of the PSS. The first of these is based on conventional spectral analysis, from which it is easy to comprehend the basic principle on which the PSS is based, and to investigate topics such as the optimum choice of PSS switching characteristics: this will be considered in Section 4. For an investigation of the optimum choice of the switched sheet impedances and its influence on PSS bandwidth, however, a circuit description, based on a transmission-line analysis (TLA), is probably more useful, and will be considered in Section 3. This approach is valid for both CW and pulsed incident signals, since the duration of a radar pulse is very long compared with the wave transit time through the PSS structure, and compared to the time for one half-cycle of the switching waveform used to control the active layer(s) in the PSS.

## 3. TLA Analysis of the Single-Active-Layer PSS

The transmission-line analog of a typical single-active-layer PSS is shown in Figure 2. It consists of a short-circuited length,  $d$ , of transmission line, with characteristic admittance  $Y_c$  and propagation constant  $\beta$ . A time-varying admittance,  $Y(t)$ , across is placed across the input terminals of the transmission line, where  $Y(t)$  is defined to be

$$Y(t) = Y_1, \quad 0 < t < \tau, \quad (1)$$

$$Y(t) = Y_2, \quad \tau < t < T,$$

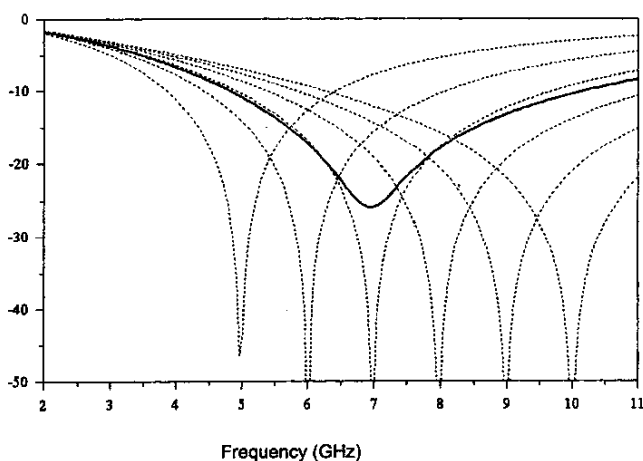


Figure 1. The predicted time-averaged reflectivity (vertical axis, in dB) characteristics of active RAM over a wide bandwidth: the dotted line is for a slow tuning rate; the solid line is for a fast tuning rate.

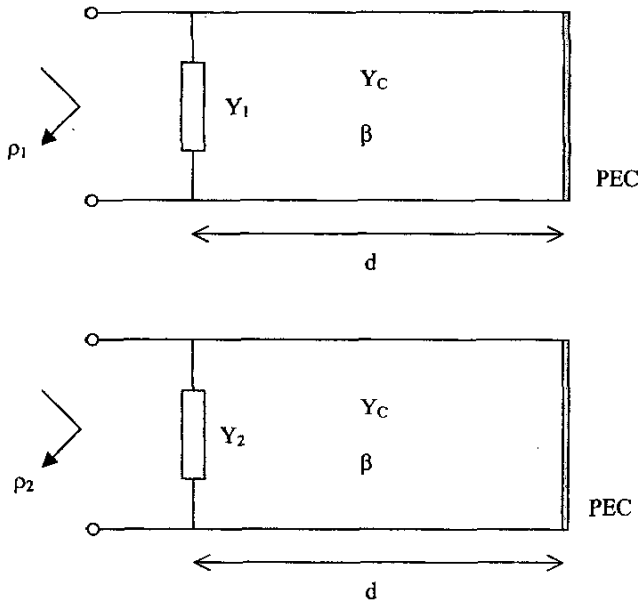


Figure 2. A short-circuited transmission line shunted by a time-varying conductance

where  $\tau$  is the “on” time and  $T$  is the time period for one cycle of the waveform used to control the state of  $Y(t)$ . Depending on the incident polarization and angle of incidence,  $\theta$ ,  $Y_c$  is given either by  $Y_c = \frac{Y_0}{\cos\theta}$  for parallel polarization, or  $Y_c = Y_0 \cos\theta$  for perpendicular polarization. For either polarization,  $\beta$  is given by  $\beta = \beta_0 \cos\theta$ . Thus, the input admittance of the PSS can assume one of two states, either  $Y_{in1}$  or  $Y_{in2}$ , given by

$$Y_{in1} = Y_1 - jY_c \cot \beta d, \quad (2)$$

$$Y_{in2} = Y_2 - jY_c \cot \beta d.$$

These result in reflection coefficients  $\rho_1$  and  $\rho_2$ , which are related to  $Y_{in1}$  and  $Y_{in2}$  by

$$\rho_1 = \frac{(Y - Y_{in1})}{(Y + Y_{in1})}, \quad (3)$$

$$\rho_2 = \frac{(Y - Y_{in2})}{(Y + Y_{in2})},$$

where  $Y = \frac{Y_0}{\cos\theta}$  or  $Y_0 \cos\theta$  for parallel or perpendicular polarization, respectively. Since  $Y_{in1}$  and  $Y_{in2}$  are arbitrary, then  $\rho_1$  and  $\rho_2$  are generally complex.

For the PSS to behave like a perfect absorber at a particular frequency, then the reflection coefficient,  $\rho$ , when averaged over time  $T$ , must be equal to zero, i.e.,

$$\rho = \frac{1}{T} \int_0^T \rho dt = \frac{1}{T} [\tau \rho_1 + (T - \tau) \rho_2] = 0. \quad (4)$$

This leads to the general condition for the PSS, which relates  $Y_{in1}$  and  $Y_{in2}$  to  $Y_0$ . Thus, from Equations (3) and (4),

(a) parallel polarization

$$Y_{in1} Y_{in2} + \frac{Y_0}{\cos\theta} \left(1 - \frac{2\tau}{T}\right) (Y_{in2} - Y_{in1}) = \frac{Y_0^2}{\cos^2\theta}, \quad (5)$$

(b) perpendicular polarization

$$Y_{in1} Y_{in2} + Y_0 \cos\theta \left(1 - \frac{2\tau}{T}\right) (Y_{in2} - Y_{in1}) = Y_0^2 \cos^2\theta. \quad (6)$$

In the simplest case, when  $\tau = T/2$ , Equations (5) and (6) simplify to

$$Y_{in1} Y_{in2} = \frac{Y_0^2}{\cos^2\theta}, \quad (7)$$

$$Y_{in1} Y_{in2} = Y_0^2 \cos^2\theta,$$

or when written in terms of the switched admittances,  $Y_1$  and  $Y_2$ ,

(a) parallel polarization

$$\left[ Y_1 - j \frac{Y_0}{\cos\theta} \cot(\beta_0 d \cos\theta) \right] \left[ Y_2 - j \frac{Y_0}{\cos\theta} \cot(\beta_0 d \cos\theta) \right] = \frac{Y_0^2}{\cos^2\theta}, \quad (8)$$

(b) perpendicular polarization

$$\left[ Y_1 - j Y_0 \cos\theta \cot(\beta_0 d \cos\theta) \right] \left[ Y_2 - j Y_0 \cos\theta \cot(\beta_0 d \cos\theta) \right] = Y_0^2 \cos^2\theta. \quad (9)$$

If the incident frequency,  $f_c$ , is such that  $d \cos\theta = \frac{\lambda_c}{4}$ , then

$\beta_0 d \cos\theta = \frac{\pi}{2}$ , and Equations (8) and (9) simplify to

$$Y_1 Y_2 = \frac{Y_0^2}{\cos^2\theta}, \quad (10)$$

$$Y_1 Y_2 = Y_0^2 \cos^2\theta. \quad (11)$$

Since the time-averaged reflection coefficient,  $\rho$ , is zero, the PSS behaves like a perfect absorber at  $f_c$ , as expected. When  $d \cos\theta \neq \frac{\lambda_c}{4}$ ,  $\rho$  will not, in general, be equal to zero, but will depend on the particular form of  $Y_1$  and  $Y_2$  [23]. To simplify the discussion that follows, let  $Y_1 = G_1$ ,  $Y_2 = G_2$ , and  $\theta = 0^\circ$  (the oblique-incidence case is discussed in [24]). Then, Equations (10) and (11) both simplify to

$$R_1 R_2 = Z_0^2, \quad (12)$$

where  $R_1 = 1/G_1$ ,  $R_2 = 1/G_2$ , and  $Z_0 = 1/Y_0$ .

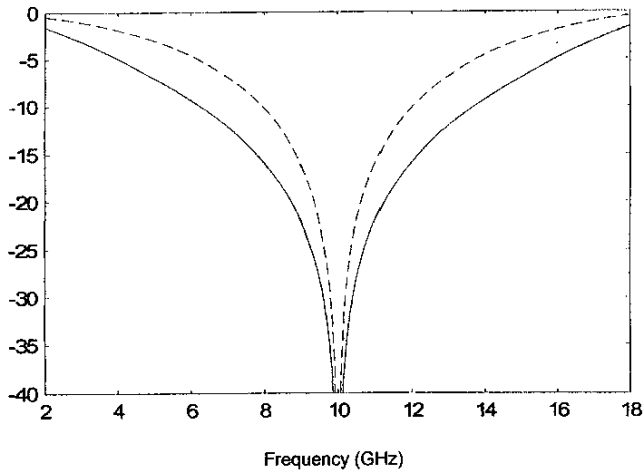


**Figure 3.** The frequency characteristics of a passive Salisbury screen (solid line) and of a single-layer planar phase-switched screen,  $d = 7.5$  mm (dashed line). The vertical axis is the reflectivity in dB.

Equation (12) has been reported previously in connection with diode-switched reflection phase shifters [25], but was derived independently for active radar absorbers in [26]. Although not mentioned in the literature, Equation (12) also applies to the passive Salisbury screen, since it relates the two possible values of front sheet resistance that give a particular reflectivity-null depth.

In principle, there is an infinite number of pairs of resistance values that will satisfy Equation (12). However, in the experimental PSS to be described later, the switched resistive layer takes the form of a frequency-selective surface (FSS), consisting of PIN-diode-loaded dipole elements that are biased either fully “on” or fully “off.” Hence, to a reasonable approximation over the bandwidth of the FSS,  $R_1 \approx 0 \Omega$  and  $R_2 \approx \infty \Omega$ . Then,  $\rho_1 \rightarrow -1$ ,  $\rho_2 \rightarrow +1$ , and the time-averaged value of  $\rho \approx 0$  as expected, since the “on” time,  $\tau = T/2$ . If the value of  $d$  is now fixed, it is easy to show that as  $f_c$  varies, then  $\rho$  varies as  $\cos \beta d$  (and, hence, reflectivity =  $20 \log_{10}(|\cos \beta d|)$ ). Figure 3 compares this frequency variation of reflectivity with that for a Salisbury screen with the same value of spacer thickness,  $d$ . It can be seen that the bandwidth of the PSS is somewhat narrower than that of the Salisbury screen, and this behavior may be explained by considering the influence of multiple reflections inside the PSS structure. When  $R_1$  and  $R_2$  only take on values of 0 or  $\infty$ , the incident wave is only reflected from either the front or the back face of the PSS, and no multiple reflections can occur. However, for other combinations of  $R_1$  and  $R_2$ , some of the energy incident on the front face of the PSS can always penetrate into its interior, thus giving rise to multiple reflections that will change the frequency characteristics. In the limiting case, when  $R_1 = R_2 = Z_0$ , then the frequency characteristics of the PSS become identical to those of the Salisbury screen.

From Figure 3, it can be seen that at resonance (i.e.,  $\beta_0 d = \pi/2$ ), the effect of switching  $R(t)$  between values  $R_1$  and  $R_2$  – as related by Equation (12) – mimics the reflectivity characteristics of a passive layer having a sheet resistance equal to  $Z_0$ . Hence, it should be possible to adjust the effective sheet resis-

tance,  $R_{eff}$ , by varying the “on” time,  $\tau$ , in each switching cycle. The relationship between  $R_{eff}$  and  $\tau$  is given by [26]

$$R_{eff} = Z_0 \frac{(T - \tau)}{\tau}, \quad (13)$$

and the dependence of the resonance-null depth of the PSS on  $\tau/T$  is shown in Figure 4. Hence, the PSS may be configured to act as a reflector or as a variable absorber, simply by changing the mark-space ratio of the control waveform applied to the switched resistance layer. This behavior is confirmed by the measured data shown in Figure 5.

The normal single-layer PSS has a switchable front layer,  $A$ , and a PEC backplane. In some applications, where the structure to be shielded from an incident wave is thin (e.g., a missile fin), it might be advantageous to replace the PEC backplane by a second switchable layer,  $B$ , thus giving rise to a bidirectional PSS (BPSS) that is effective against illumination from either side of the structure. In operation, each active layer is switched so that at successive instants in time,  $R_A = 0, R_B = \infty$ ;  $R_A = \infty, R_B = 0$ ;  $R_A = 0, R_B = \infty$ , etc. From Figure 4, it can be seen that the bidirectional PSS will then have the same apparent reflectivity when viewed from either side.

Although the transmission-line analysis of Section 3 enables us to examine the frequency characteristics of the PSS, it does not allow us to determine the optimum choice of switching-waveform shape and frequency, particularly in the presence of pulsed incident signals. This will be considered in Section 4.

#### 4. Spectral Analysis of the Single-Active-Layer PSS

For simplicity, we will consider here only the case of a single-active-layer PSS, operating against a periodic train of rectangular pulses of carrier frequency  $f_c$  [27], as shown in Fig-

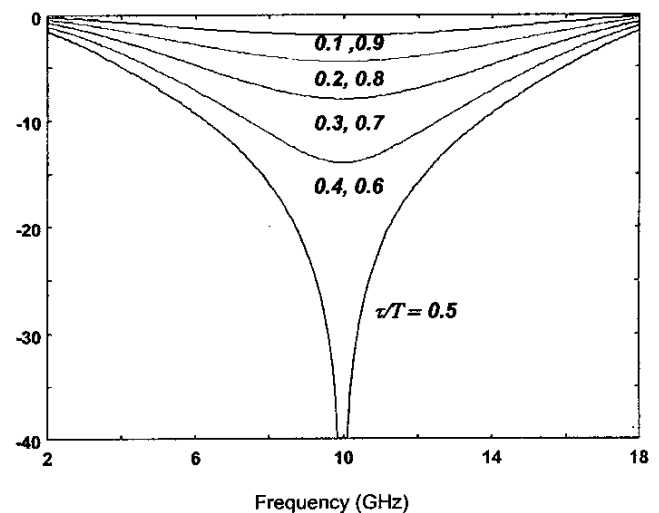


**Figure 4.** The variation of null depth with  $\tau/T$  for a resistively switched PSS. The vertical axis is the reflectivity in dB.

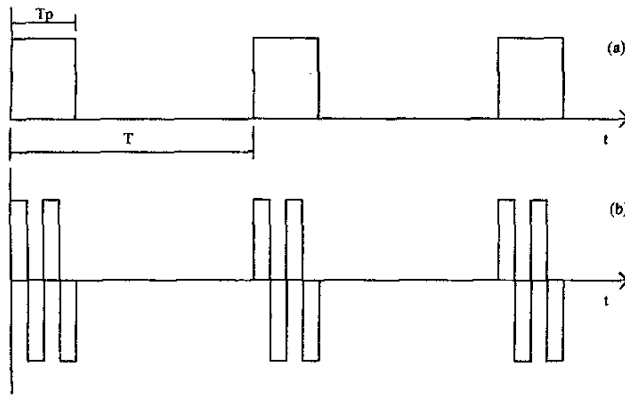


Figure 6. The operation of the phase-switched screen: (a) the incident wave; (b) the reflected wave ( $M = 2$ ; for clarity, the sinusoidal carrier-frequency signal itself is not shown).

Figure 6a. Each pulse is of length  $T_p$ , and the pulse repetition period is  $T$ . After reflection from the PSS, assume that each incident carrier pulse is replaced by  $M$  cycles of a bipolar rectangular waveform, as shown in Figure 6b. Hence, the period of this modulating waveform,  $2\tau$ , is given by

$$2\tau = \frac{T_p}{M}, \quad (14)$$

and the switching frequency,  $f_s$ , is given by  $f_s = \frac{M}{T_p}$ .

Since the incident pulse train is periodic with period  $T$ , its spectrum and that of the signal reflected from the PSS may be determined using Fourier analysis. Hence, the incident and reflected signals may be written in the form

$$v(t) = \sum_{n=-\infty}^{n=+\infty} c_n e^{jn\omega_0 t}, \quad (15)$$

where  $\omega_0 = 2\pi/T$ . The complex Fourier coefficients,  $c_n$ , are then given by

$$c_n = \frac{1}{T} \int_0^T v(t) e^{-jn\omega_0 t} dt. \quad (16)$$

For the incident periodic pulse train, the  $c_n$  are given by

$$c_n = \frac{-j}{2n\pi} \left( 1 - e^{-j2n\pi \frac{T_p}{T}} \right). \quad (17)$$

For the PSS-modulated wave and  $M$  an integer,  $c_n$  may be written in the form

$$c_n = \frac{j}{2n\pi} \zeta \chi \sum_{m=1}^M e^{-2\gamma(m-1)}, \quad (18)$$

where

$$\gamma = jn\omega_0 \tau, \quad (19)$$

$$\zeta = 1 - e^{-\gamma}, \quad (20)$$

$$\chi = \left( e^{j2\beta d} + e^{-\gamma} \right), \quad (21)$$

and

$$\beta = \frac{2\pi}{\lambda}. \quad (22)$$

In the general case of non-integer  $M$ , Equation (18) is modified to

$$(a) \quad M = M + \delta M, \quad 0 \leq \delta M \leq 1/2,$$

$$c_n = \frac{j}{2n\pi} \left[ \zeta \chi \sum_{m=1}^M e^{-2(m-1)\gamma} + e^{j2\beta d} e^{-2M\gamma} \left( 1 - e^{-\frac{\gamma x}{\tau}} \right) \right], \quad 0 \leq x \leq \tau, \quad (23)$$

$$(b) \quad M = M + \delta M, \quad 1/2 \leq \delta M \leq 1,$$

$$c_n = \frac{j}{2n\pi} \left[ \zeta \chi \sum_{m=1}^M e^{-2(m-1)\gamma} + \zeta e^{j2\beta d} e^{-2M\gamma} + e^{-(2M+1)\gamma} \right] \left( 1 - e^{-\frac{\gamma y}{\tau}} \right), \quad 0 \leq y \leq \tau. \quad (24)$$

It should be noted that Equations (18)-(24) actually give the spectral components of the incident and PSS-modulated signals relative to the carrier frequency, i.e., the component  $c_0$  is actually at  $f_c$ . The apparent PSS reflectivity at frequency  $f_c$ , for any switching frequency  $f_s$ , may now be found by comparing how much energy would enter the receiver pass-band in the absence of PSS modulation and when PSS modulation has taken place. In the discussion of results that follow, it is assumed that for a pulse-width  $T_p$ , the receiver has a total bandwidth of  $2/T_p$ , since this is consistent with the generally accepted rule of thumb that the receiver bandwidth at the 3 dB points is given approximately by  $B = 1/T_p$ .

Equations (18)-(24) were used initially to calculate the apparent reflectivity of a resonant (i.e.,  $d = \lambda/4$ ) PSS when the incident signal was a periodic train of 1  $\mu$ sec rectangular pulses of sinusoidal carrier with  $f_c = 10$  GHz and a pulse duty cycle of 1%. The resulting curve of reflectivity as a function of switching frequency is shown in Figure 7 and, as expected, the PSS effective reflectivity decreases with increasing switching frequency. When the PSS is in a non-resonant condition ( $d \neq \lambda/4$ ), then it presents periodic reflection coefficients of  $-1$  (active layer on,  $R(t) = 0$ ) and  $-e^{j2\beta d}$  (active layer off,  $R(t) = \infty$ ) to the incident signal. The other two curves in Figure 7 show the PSS reflectivity performance for incident signals at frequencies of 11 GHz and 15 GHz. These curves are identical to those for incident signals at 9 GHz and 5 GHz, respectively, thus confirming the symmetrical nature of the PSS frequency response. It should also be noted that for high val-

ues of switching frequency, the predicted values of PSS reflectivity agree with those calculated from  $20\log_{10}(|\cos \beta d|)$ . The results shown in Figure 7 may be scaled so that they are applicable to other pulse widths and receiver bandwidths. For example, if the pulse width is decreased by a factor of 10, then the receiver bandwidth and the switching frequency must be increased by the same factor to give the same value of reflectivity as before.

Consider now the spectrum of the PSS-modulated signal. Figure 8 compares the spectrum of an incident signal, composed of a train of 1  $\mu\text{sec}$  pulses of carrier frequency 10 GHz and duty cycle of 1%, with that of a signal reflected from a PSS the reflection coefficient of which is switched between  $\pm 1$  using an 8 MHz bipolar square waveform. It can be seen that the level of the signal reflected at  $f_c$  has been reduced considerably, and that the energy originally at  $f_c$  has been redistributed mainly amongst the sidebands positioned at  $f_c \pm 8n$  MHz,  $n$  odd. Figure 9 shows the corre-

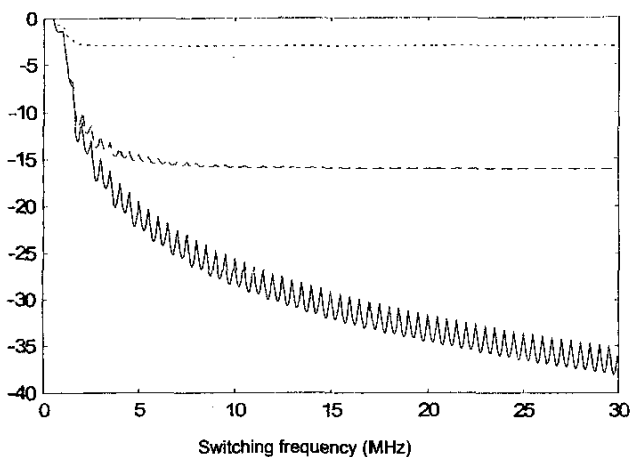


Figure 7. The reflectivity (vertical axis, in dB) of a planar single-layer PSS with 1:1 bipolar square-wave switching: 1  $\mu\text{sec}$  pulse length, 1% duty cycle, 2 MHz receiver bandwidth. —  $f_c = 10$  GHz, ---  $f_c = 11$  GHz,  $\cdots$   $f_c = 15$  GHz.

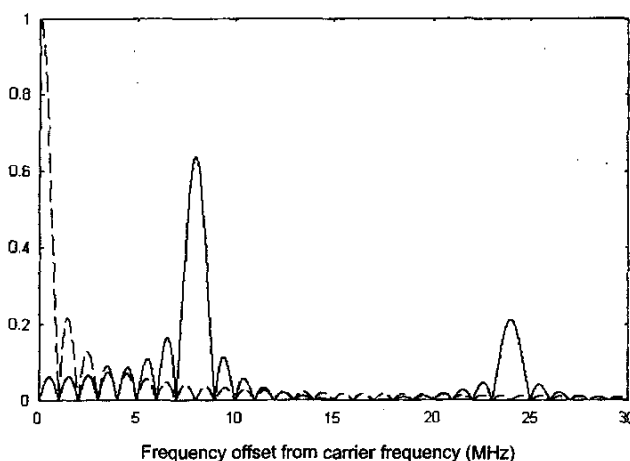


Figure 8. The one-sided frequency spectrum of a pulsed carrier signal incident on and reflected from a PSS switched at 8 MHz:  $f_c = 10$  GHz, 1  $\mu\text{sec}$  pulses, 1% pulse duty cycle; --- incident signal, — reflected signal. The vertical axis is the normalized spectrum amplitude.

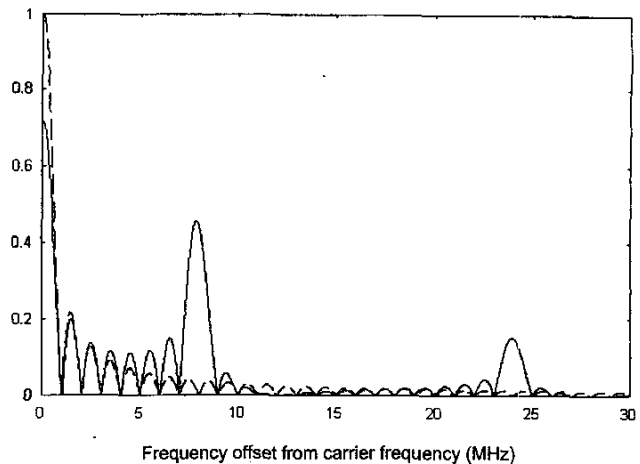


Figure 9. The one-sided frequency spectrum of a pulsed carrier signal incident on and reflected from a PSS switched at 8 MHz:  $f_c = 15$  GHz, 1  $\mu\text{sec}$  pulses, 1% pulse duty cycle; --- incident signal, — reflected signal. The vertical axis is the normalized spectrum amplitude.

sponding spectrum when the signal incident on the same PSS is at a frequency of 15 GHz. In this case, less energy is redistributed from around  $f_c$  into the sidebands, and so the resulting apparent reflectivity performance is worse than that at 10 GHz. Experimental confirmation of the spectral spreading provided by the PSS is shown in Figure 10. In this case, a single-active-layer PSS, optimized for use at 11 GHz and operating in free space, was illuminated by a pulsed 11 GHz plane-wave signal (1  $\mu\text{s}$  pulses with 0.1% duty cycle), and the PSS was switched at 20 MHz. Hence, from Figure 10, a receiver with a 2 MHz bandwidth would “see” the PSS as exhibiting a reflectivity of less than  $-30$  dB, which is in good agreement with the predictions for the 10 GHz optimized PSS when also switched at 20 MHz, as shown in Figure 7.

Returning now to Figure 8, if the PSS was being used to reduce the apparent radar cross section of an object, a possible countermeasure might be to use a wideband receiver to detect the reflected spectral components at  $f_c \pm 8$  MHz. An obvious method of avoiding this would be to increase the PSS switching frequency,  $f_s$ , but if the PSS surface was electrically large and  $f_s$  was high enough, this might cause EMC problems or the PSS might even act as a beacon at  $f_s$  or its harmonics. Careful design and layout of the PSS surface should avoid these problems (see also Section 9.2), but here we look briefly at a solution involving spectrum-spreading techniques, whereby the 8 MHz sidebands are broadened out by switching the PSS reflection coefficient in a non-periodic manner. Because such cases are not easily amenable to analytical solution using the previous Fourier-analysis technique, all the results to be discussed from now on were obtained numerically, using the FFT.

The sideband energy in the PSS-reflected signal may be spread out by changing the effective PSS switching frequency within the period of one radar pulse. For example, the upper curve in Figure 11 shows the effect of switching using a waveform that has been generated by choosing consecutive 16-bit strings (since the nominal switching frequency of 8 MHz is equivalent to 16 half-cycles within the 1  $\mu\text{sec}$  radar pulse) from the primitive polynomial (modulo 2) sequence, of order 11 [28]. The overall  $m$  sequence is  $2047 (2^{11} - 1)$  bits long, to which has been added an additional 0 bit, so as to equalize the number of 1s and 0s (to

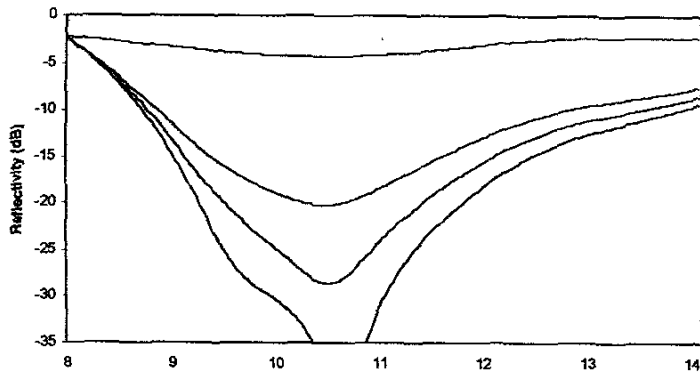


Figure 5. The measured variation of the null depth for a resistively switched single-active-layer PSS.

Figure 10. The measured free-space frequency spectra of pulsed incident and PSS-reflected signals. The incident carrier frequency and PSS center frequency were 11 GHz, the pulse length was 1  $\mu$ sec, the duty cycle was 0.1%, and the PSS switching frequency was 20 MHz. The incident signal is in yellow, and the reflected signal is in cyan.

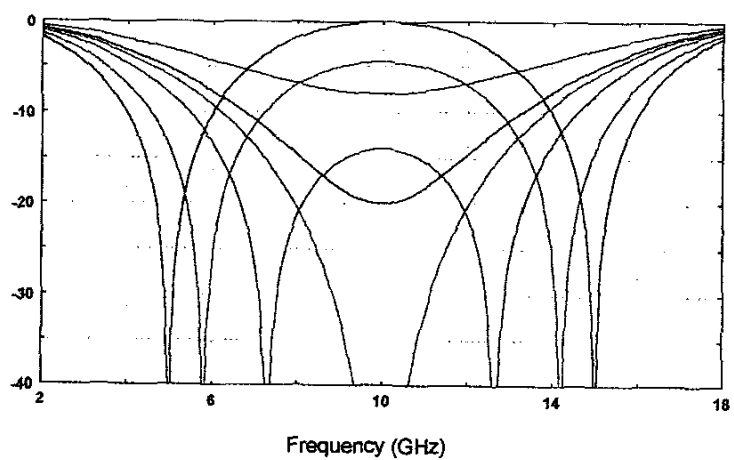
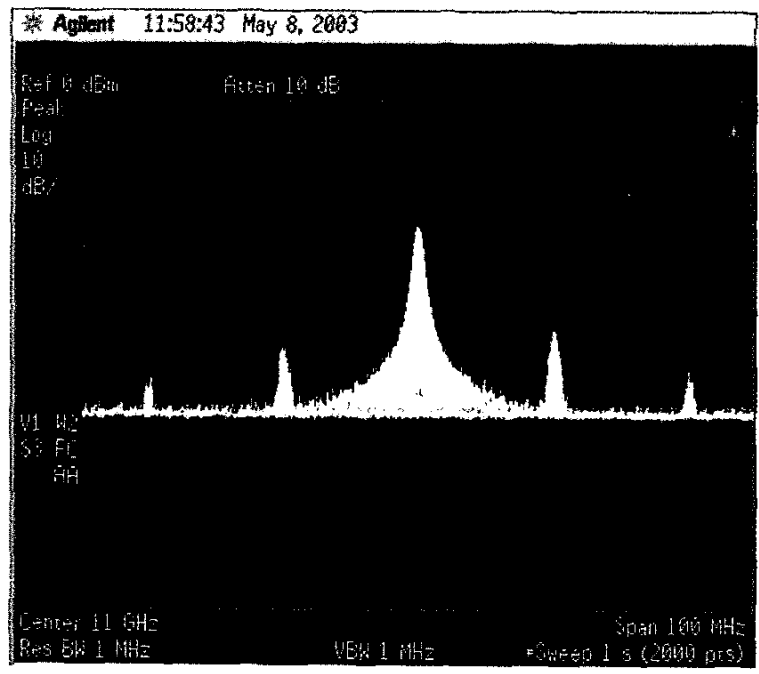
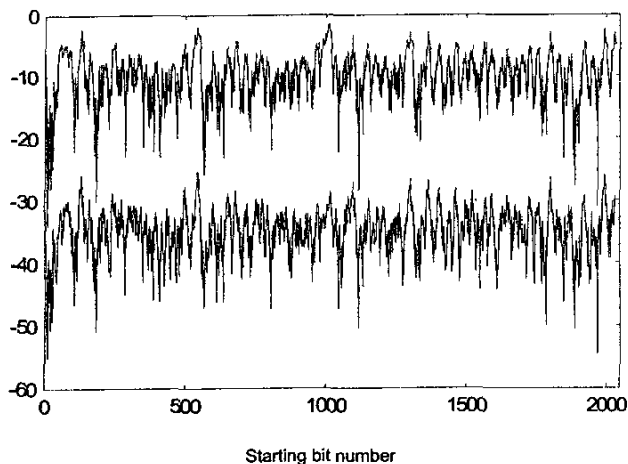


Figure 24. The control of the null position and depth in a two-active-layer PSS by varying the layer "on" times. The vertical axis is the reflectivity in dB.

$a_1$  0 0.2 0.4 0.5 0.55 0.7





**Figure 11.** The variation in PSS reflectivity (vertical axis, in dB) as the 16-bit switching sequence contained within the width of a 1  $\mu$ sec radar pulse was chosen sequentially from an overall switching sequence of 2048 bits. The top curve shows bipolar switching based directly on the bit sequence generated by an 11th-order polynomial (modulo 2) (mean reflectivity value = -10.2 dB). The bottom curve is the same as the top curve, but when Manchester encoding was used (mean reflectivity value = -35.1 dB).

ensure a zero dc level and, hence, zero reflected energy at  $f_c$ ). A further refinement is to then represent each 1 or 0 in the bit sequence using Manchester encoding. This breaks up local repeated occurrences of 1s or 0s in the sequence, thus smoothing out the spectrum, as well as increasing the effective switching frequency to approximately 16 MHz. The benefits of including this additional process may be seen by comparing the upper and lower curves shown in Figure 11.

Although in practice better switching strategies and higher switching frequencies would be used, it should be noted that the form of optimum spreading codes for use with a PSS might differ considerably from that of those used in spread-spectrum communications. There are two reasons for this. Firstly, because it is highly undesirable for an unauthorized recipient of a PSS-modulated signal to be able to reconstruct the switching sequence and so “unmask” a PSS-shielded object through appropriate signal processing in the receiver, the autocorrelation properties of the PSS switching sequence must be designed to protect against this. Secondly, it is highly desirable for the number of 1s and 0s in those portions of the PSS switching sequence that are used while radar pulses are actually illuminating the PSS be equal or nearly so, since this ensures good suppression of the incident carrier-frequency component,  $f_c$ , by the PSS. For this reason, switching sequences generated using primitive polynomials alone are not suitable, because of their inherently poor localized distribution of 1s and 0s. Herein lies the advantage of additional Manchester encoding, since this condition is then automatically fulfilled [27].

## 5. Reactive Single-Active-Layer PSS

The discussion so far has considered a PSS with a single active layer that can be switched between two values of surface resistance, which are related by Equation (12). A limitation of this

structure is that it can only provide a single reflectivity null with a limited bandwidth. However, the bandwidth can be increased significantly if the active layer is reactive. This approach is similar to that used in the design of passive-circuit analog absorbers, where a reactive impedance sheet is used to counteract the change in electrical-spacer thickness with frequency [6].

It can be shown that a PSS with a single active layer, which is switched between reactance values of  $\pm jZ_0 \sin \beta_0 d$  by an equal-mark-space-ratio square wave, has zero time-averaged reflectivity over a frequency band defined by  $0 < \beta_0 d < \pi$ . For example, a 5 mm-thick air-spaced PSS could, theoretically, exhibit zero reflectivity from 0 to 30 GHz. In terms of a circuit analog, the active layer is switched between inductive and capacitive reactance states described by  $Z_1 = j\omega L$  and  $Z_2 = 1/j\omega C$ . Here, both  $L$  and  $C$  are functions of frequency, as shown in Figure 12, and are such that they are resonant at all frequencies within the operating band, i.e.,  $f = 1/2\pi\sqrt{LC}$ . Although such a reactive layer is not physically realizable using currently known materials, the use of reactive impedance switching can nevertheless significantly increase the bandwidth of a PSS, as shown by the measured data in Figure 5 and the following theoretical examples. The first case to be examined is that in which the impedance layer is switched between two states that correspond to fixed values of inductance and capacitance, i.e.,  $Z_1 = j\omega L_1$  and  $Z_2 = 1/j\omega C_1$ . Figure 13 shows the reflectivity characteristics of a 5 mm-thick air-spaced PSS for which  $L_1 = 10$  nH and  $C_1 = 64.5$  fF. In this example, the values of capacitance and inductance have been chosen to optimize the -20 dB reflectivity bandwidth.

A closer approximation to the impedance states of the ideal active layer,  $Z_{1,2} = \pm jZ_0 \sin \beta_0 d$ , can be achieved over a limited bandwidth by using a layer that contains both inductance and

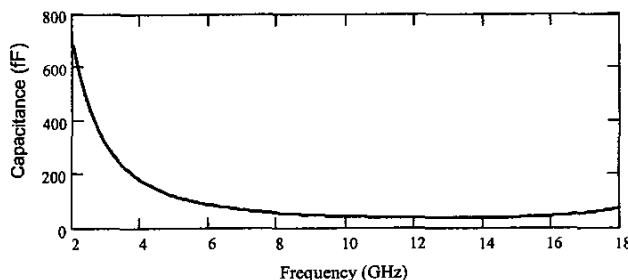


**Figure 12a.** The capacitance of a PSS active layer required to give zero reflectivity.

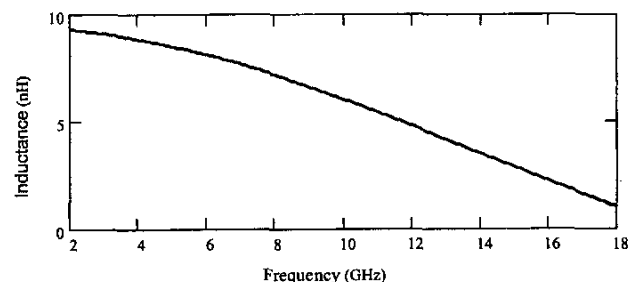


**Figure 12b.** The inductance of a PSS active layer required to give zero reflectivity.

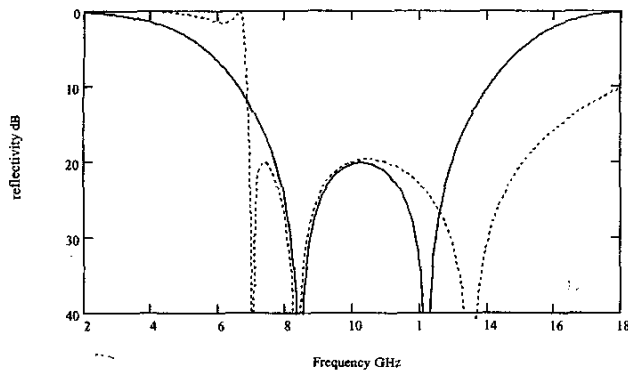


Figure 13. The predicted reflectivity characteristics of a switched-reactance single-layer PSS: —  $d = 5$  mm,  $L_1 = 10$  nH,  $C_1 = 64.5$  fF; - - -  $d = 5$  mm,  $L_1 = 0.975$  nH,  $C_1 = 72$  fF,  $L_2 = 94$  nH,  $C_2 = 5.7$  fF.

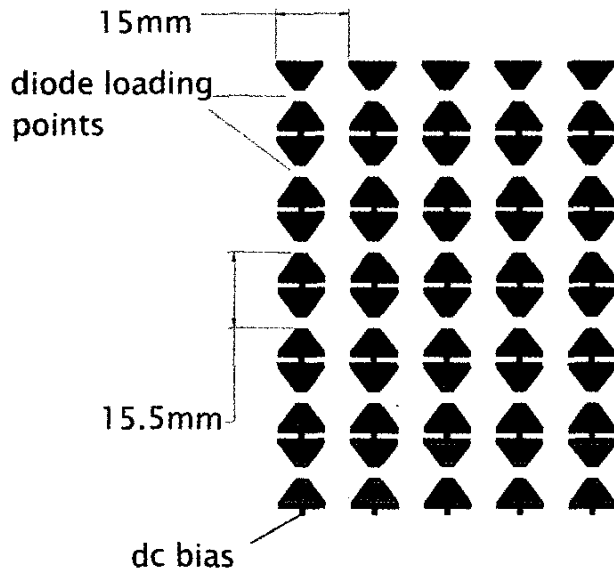


Figure 14a. The layout of the PSS active layer.

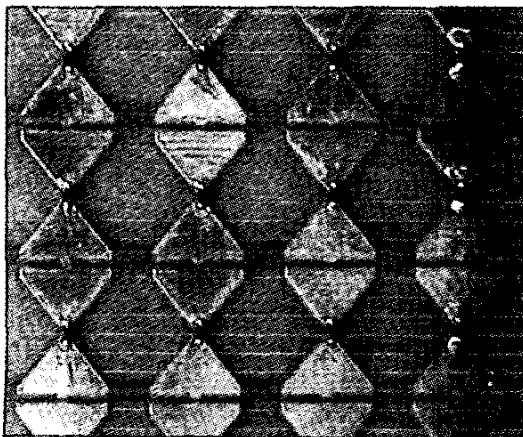


Figure 14b. A photo of the PSS active layer.

capacitance, i.e.,  $Z_1 = j\omega L_1 + 1/j\omega C_1$  and  $Z_2 = j\omega L_2 + 1/j\omega C_2$ . Using this approach, the reflectivity bandwidth of the PSS considered in the previous example can be increased to provide a response of at least  $-20$  dB over more than one octave. A second design is also shown in Figure 13, for which  $L_1 = 0.975$  nH,  $C_1 = 72$  fF, and  $L_2 = 94$  nH,  $C_2 = 5.7$  fF. This now raises the question as to how reactance can be incorporated into the active layer. In our layers, reactance is always present by default, since the former are based on switchable frequency-selective surfaces that are controlled by PIN diodes.

## 6. How to Build a PSS

To realize a practical PSS, we need a surface that can be rapidly switched between two or more impedance states. Potentially this could be achieved using some type of functional material, such as an active conducting polymer [9], but to date we have concentrated on the development of layers comprised of a two-dimensional grid of half-wavelength dipoles that are loaded at their centers with PIN diodes. Under no-bias conditions, the PIN diodes present high microwave impedance, and the dipoles may be considered open circuit. Hence, the grid of dipoles is nonresonant, and represents a high-impedance equivalent surface. When the diodes are biased "on," however, their microwave impedance becomes low, and the dipoles are resonant at the half-wavelength frequency. Then, the grid of shorted dipoles becomes a strong scatterer, and represents a low-impedance surface. The basic geometry of the active layer in our PSSes is shown in Figure 14 [29]. The layer is based on a unit cell containing a bowtie dipole, which is loaded at its center by a PIN diode contained in an SOD323 package. In order to connect adjacent diodes in series strings, each dipole has a short tab at one end, and this also serves to add a controlled amount of inductance to the circuit, so as to broaden its frequency response. Also shown in Figure 14 is a close-up view of part of an active layer containing 900 elements.

## 7. Dual-Polarized PSS

The practical PSS design discussed in Section 6 is only sensitive to a single linear incident polarization. In most operational situations, however, a dual-polarized PSS would be advantageous. In this section, we describe some of our initial work on the design of a dual-polarized screen. An obvious approach to the design of a dual-polarized active layer would be to fabricate two linearly polarized dipole-grid arrays, arranged on opposite sides of a thin substrate. However, a problem with this approach is that although the substrate can be made very thin (10 microns) – using, for example, a Mylar substrate – the surface-mount PIN diode packages that we currently use are approximately 1 mm high. This results in different effective electrical spacings between the backplane and the two active layers. Hence, we are investigating an alternative topology, which combines two orthogonal grids of bowtie-dipole elements along with an integrated diode feed network that can be fabricated on a single-sided printed-circuit board, as shown in Figure 15 [30].

To test the dual-polarized design, a synthesis procedure was employed in which two FSSes with open-circuit and short-circuit conditions at the diode-loading points were used to represent an active PIN-diode-loaded FSS under bias and no-bias conditions. A loose-lay PSS configuration was constructed by mounting the FSS above an aluminum conducting backplane, using an 8 mm thick,

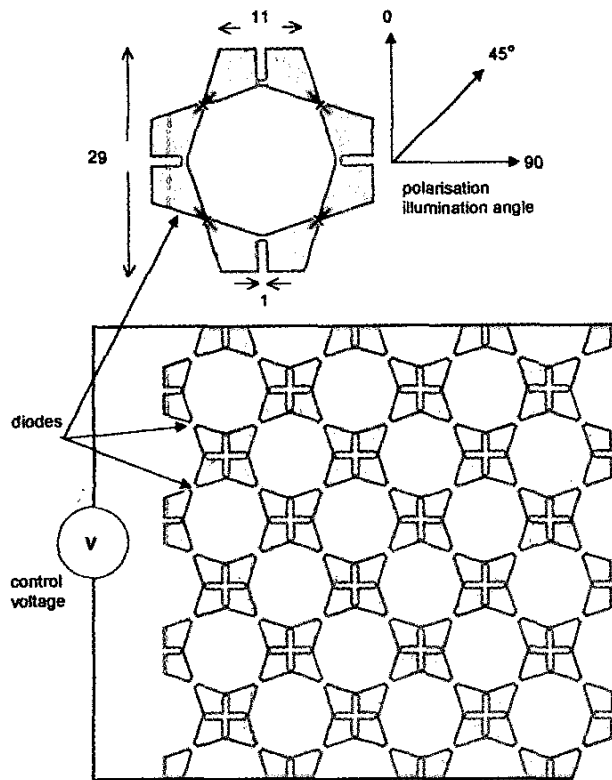


Figure 15. The details of the dual-polarized active-surface unit-cell geometry (all dimensions in mm), and a representation of the grid layout.

low-loss, foam dielectric spacer ( $\epsilon_r = 1.05$ ,  $\tan \delta = 0.0017$ ). Complex reflectivity data were measured for this loose-lay configuration over a frequency range of 2-12 GHz for linear incident polarization at rotation angles of  $0^\circ$ ,  $45^\circ$ , and  $90^\circ$ , respectively. For each measurement, two data sets were recorded: one with the loose-lay PSS containing the open-circuit FSS, and the other with the short-circuit FSS. The measured data were then used to synthesize the reflectivity performance of an active PSS modulated by a periodic square wave by combining the data using Equation (4), where  $\rho_1$  and  $\rho_2$  represent the complex reflection coefficients of the PSS measured with the open-circuit and short-circuit FSSes, respectively. The synthesized reflectivity response of the PSS at polarization angles of  $0^\circ$ ,  $45^\circ$ , and  $90^\circ$  are presented in Figure 16. The bandwidth response of this prototype dual-polarized design is compared to that of the linear screens, and we are currently working on new FSS topologies to provide a wideband response.

## 8. Conformal PSS

In many practical situations where RCS (radar cross section) control is an issue, the object under consideration will not be planar, and any coating, or screening structure, will need to conform to the geometry of the object. As a first step towards this problem, we now briefly examine the application of PSS techniques to cylindrical surfaces. A theoretical description of some of the design issues relating to a cylindrical PSS may be found in previously published work [31, 32], so here we restrict the discussion to a report of our experimental work.

As in the planar PSS designs, the active surface has been formed from a periodic grid of PIN-diode-loaded bowtie dipoles. However, to allow closer packing of the elements on the grid (necessary because of the small radius of the particular PSS design presented here), the flare angle of the bowtie dipole was reduced. To allow the formation of the cylindrical PSS geometry, the active surface was fabricated on a flexible Mylar substrate. An experimental cylindrical PSS was formed, using a 120 mm-long, 16 mm-radius aluminum bar as "the backplane." The dielectric spacer consisted of a Perspex tube ( $\epsilon_r = 2.6$ ), with inner and outer radii of 16 mm

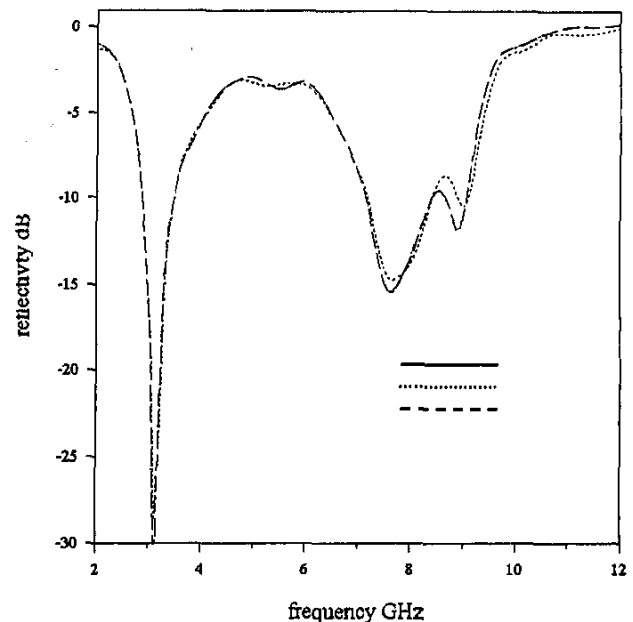


Figure 16a. The reflectivity response of the dual-polarized active PSS, synthesized from measured data ( $\tau = 0.42$ ).

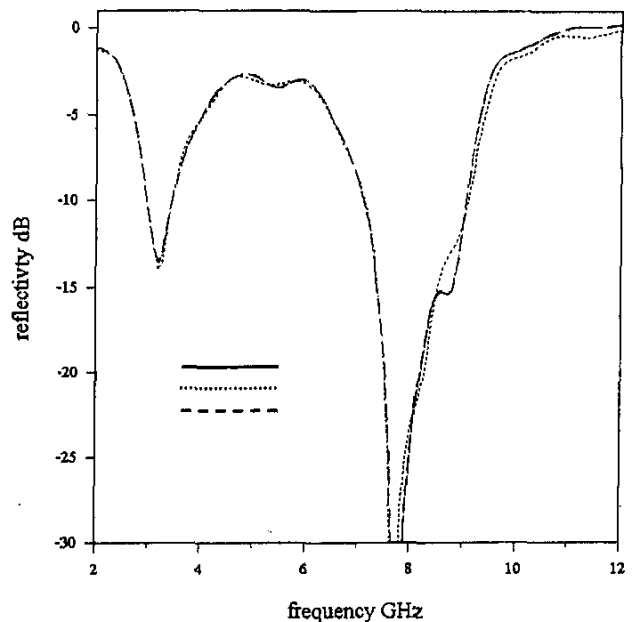


Figure 16b. The reflectivity response of the dual-polarized active PSS, synthesized from measured data ( $\tau = 0.54$ ).

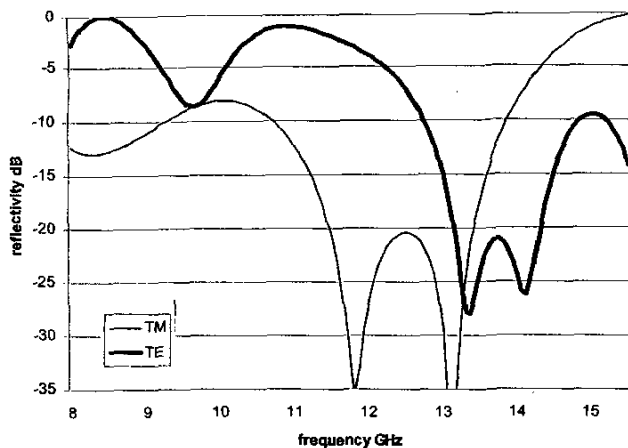


Figure 17. The measured reflectivity response of the cylindrical PSS.

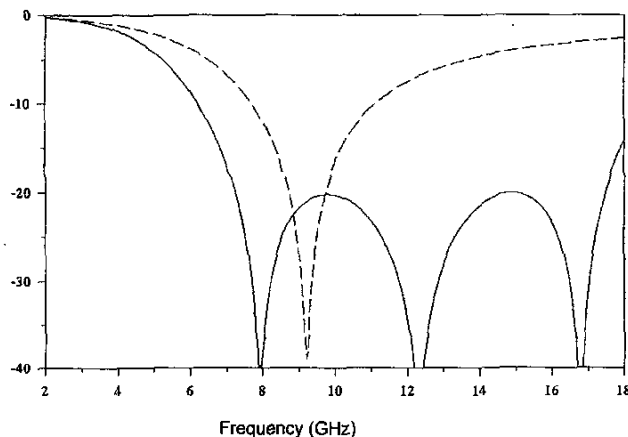


Figure 18. The reflectivity (vertical axis, in dB) characteristics of a skinned (solid) and an un-skinned (dashed) single-active-layer PSS. The thickness of the skinned PSS was 8.7 mm; the thickness of the un-skinned PSS was 6.25 mm.

and 21 mm, respectively, providing an electrical spacer thickness of approximately 8.0 mm. The complete PSS structure was formed by wrapping the flexible active surface around the spacer, with the surface-mount PIN diodes facing outwards. As the active surface was designed for linear polarization only, two configurations were used to test both TE and TM illumination. For the TM PSS, the bowtie dipoles of the active surface were arranged parallel to the cylinder axis. For TE illumination, the dipoles were perpendicular to the cylinder axis.

Figure 17 shows the measured reflectivity responses of the TE and TM PSSes (these curves are referenced with respect to the bare aluminum cylindrical backplane). In both cases, a reflectivity null of less than  $-20$  dB was achieved over bandwidth greater than 1 GHz. The null response of the TE PSS occurred at a higher frequency than that of the corresponding TM PSS, and this result is consistent with the theoretical predictions presented in [29, 30] for a cylindrical PSS of relatively small radius. However, the differences may also in part be due to the different impedances presented by the TE- and TM-configured active layers, but this has yet to be investigated.

## 9. Other Types of Single-Active-Layer PSS

### 9.1 Skinned PSS

A well-known technique for improving the bandwidth of the Salisbury screen is to place a thin, high-permittivity skin in front of the resistive layer [33]. The skin not only introduces additional multiple reflections within the absorber structure, but it also protects the resistive layer from mechanical or environmental damage. The same technique can also be used with the PSS, and Figure 18 compares the predicted reflectivity performances of a skinned and an un-skinned single-active-layer PSS. It can be seen that the presence of the skin is very beneficial in terms of increased bandwidth, for only a modest increase in thickness.

### 9.2 Double Diode Switching Elements

Earlier, we discussed how the signal reflected from a single-active-layer PSS could be spread using appropriate pseudo-random binary switching sequences. Here, however, we consider an extension to the technique that uses only a simple periodic switching voltage. If the frequency of the latter is made very high, so as to move the first sideband frequencies well away from the incident carrier frequency, then problems may arise when the surface area of the PSS is electrically large. These are due to propagation effects in the PIN-diode-biasing network, and the fact that the PSS may start to radiate at the switching frequency or its harmonics. Hence, what is required is a technique for achieving the beneficial effects of a high switching frequency without the associated penalties. One promising solution is to replace the single PIN diode at the center of each dipole in the PSS active layer by two diodes, arranged as an anti-parallel pair [34]. This arrangement of diodes was first suggested in [35] for use as a millimeter-wave harmonic mixer, in which the local oscillator signal is supplied as a sub-multiple (typically, one-half) of the wanted frequency. In the case of the PSS, the voltage stimulus waveform takes the place of the local oscillator signal, but the net effect is the same. The spectrum of the signal scattered from the modified PSS should contain only sideband components at even harmonics of the switching frequency. Hence, the double-diode PSS performs as though the switching frequency has been doubled, as compared to that of the single-diode case. It should be noted that for this arrangement to operate correctly, the voltage stimulus applied to the PIN diodes in the PSS active layer now takes the form of a bipolar sine wave, rather than the square wave used previously. As an illustration of this technique, Figures 19 and 20 show the measured free-space spectrum of a signal reflected from a large-area PSS panel, operating at 10.44 GHz, the dipoles of which are center-loaded by an anti-parallel diode pair contained in a single SOD323 package.

Figure 19 shows the effect of operating the new PSS under non-optimum conditions. Even though the sine-wave voltage stimulus is adjusted correctly and frequency doubling of the switching frequency is evident in the reflected spectrum, the latter still contains a large-amplitude component at the incident carrier frequency. This may be explained by considering the time-averaged reflectivity of a finite-area single-layer PSS,  $\rho_{av}$ , to be composed of two components associated with the ON and OFF states. Hence,  $\rho_{av}$  is of the form  $\rho_{av} = \rho_{ON}\tau_{ON}S_{ON} + \rho_{OFF}\tau_{OFF}S_{OFF}$ , where  $\tau$  is the normalized time associated with a particular PSS state, and  $S$  is the effective reflecting surface area, including edge-diffraction effects. For symmetrical switching,  $\tau_{ON} = \tau_{OFF}$  and,

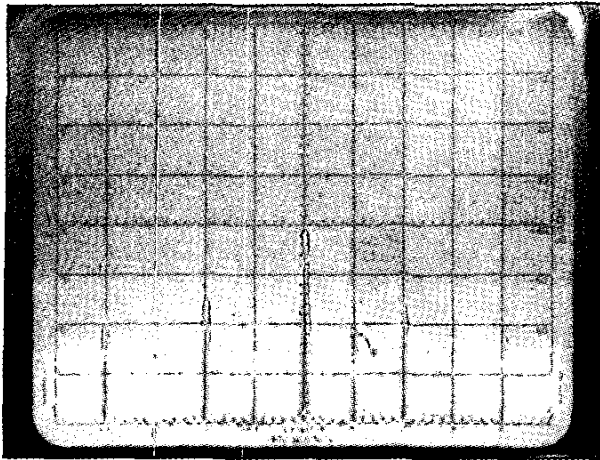


Figure 19. The spectrum of the signal reflected from a PSS with two diodes per array element.  $S_{OFF}$  and  $S_{ON}$  were not balanced, the switching frequency was 5 MHz, and the vertical scale is 10 dB/div.

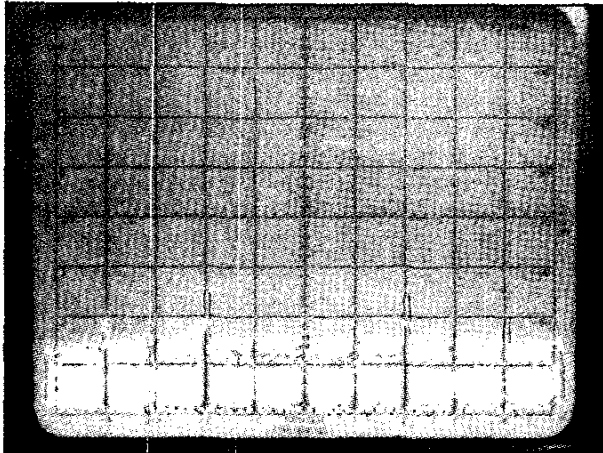


Figure 20. The Spectrum of the signal reflected from a PSS with two diodes per array element.  $S_{OFF}$  and  $S_{ON}$  were balanced, the switching frequency was 5 MHz, and the vertical scale is 10 dB/div.

hence,  $\rho_{av} = \frac{\rho_{ON}S_{ON} + \rho_{OFF}S_{OFF}}{2}$ . Then, even if  $\rho_{ON} = -\rho_{OFF}$ ,

$\rho_{av}$  will not be equal to zero if  $S_{ON} \neq S_{OFF}$ . In the PSS containing one diode per dipole element, this situation can be ameliorated by adjustment of the switching-waveform duty cycle, i.e., the ratio  $\tau_{ON} : \tau_{OFF}$ . In the PSS containing two diodes per dipole element, however, the switching waveform has to be symmetrical, and so  $\tau_{ON} = \tau_{OFF}$ ; therefore, if  $S_{ON} \neq S_{OFF}$ , the situation shown in Figure 19 will occur. On the other hand, Figure 20 shows the reflected signal spectrum that results when  $S_{ON}$  and  $S_{OFF}$  are balanced using the technique discussed in [36]. In this case, as expected, suppression of the incident carrier frequency does take place, and the measured spectrum of the signal scattered from the PSS also shows evidence of components associated with the doubling of the switching frequency. Hence, the substitution of the single diode in

each PSS array element by an anti-parallel diode pair is shown to be very advantageous in terms of improved absorber performance.

### 9.3. Smart PSS

As well as offering the potential to overcome the so-called Rozanov limit [8], a dynamically controllable structure such as the PSS can also enable additional “smart” functionality, such as search-and-null lock (SNL), identification-friend-or-foe (IFF), and absorb-while-scan (AWS) [16, 37, 38]. For the PSS to be made smart, it is necessary to modify its structure so as to facilitate two key requirements, namely incident-field sensing and electromag-netic reconfiguration. Specifically, what we have in mind is a structure based on the PSS that has the ability to sense the frequency of an incident wave, and to automatically place a reflectivity null of chosen depth onto that frequency so as to modify the target’s electromagnetic appearance to the incident wave. Incident-field sensing may be facilitated by making the PSS backplane “leaky,” and by incorporating some form of frequency-measuring element into the structure. The second requirement can be fulfilled by increasing the number of active layers in the PSS, thereby enabling simultaneous null-depth and position control. A TLA of the basic configuration of the smart PSS is shown in Figure 21. When viewed on a time-averaged basis, the structure behaves both as a bandpass filter and as a PSS. In practice, to place a reflectivity null at a particular threat frequency (the search-and-lock mode), the tuning elements in each half of the structure are adjusted simultaneously so as to maximize the amplitude of the incident signal that leaks through the structure. This behavior is illustrated by the resulting reflectivity- and transmission-loss curves, shown in Figure 22. Once this threat has been countered, the tuning elements in each half of the structure may be uncoupled so that a second threat frequency can be searched for, while still countering the first (the absorb-while-scan mode). Further details of this technique are given in [16, 37, 38].

### 10. Multiple-Active-Layer PSS

In the same way that multiple layers may be used in passive RAM to increase bandwidth, the use of several active layers in a

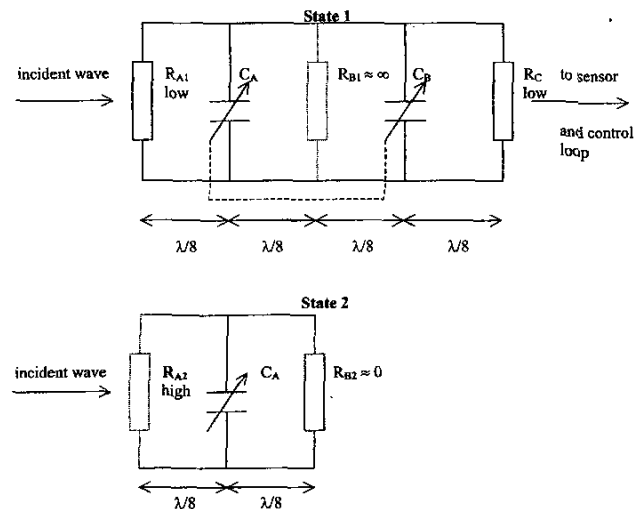
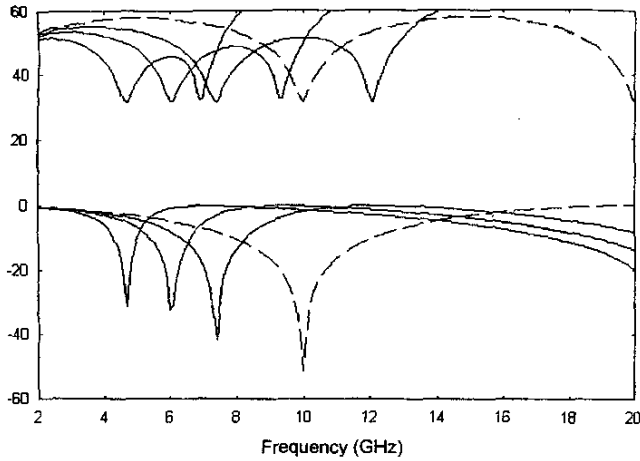
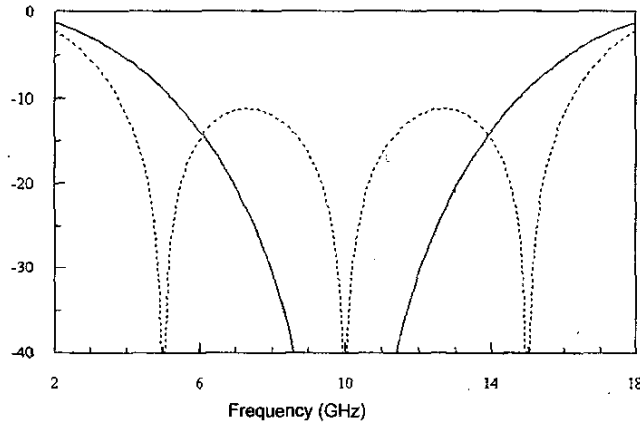


Figure 21. A tunable smart PSS structure in its two operating states.



**Figure 22.** The tuning and tracking characteristics of a smart PSS. The spacer thickness was 7.5 mm; the dashed lines are for  $C_A = C_B = 0$  fF; the solid lines are for  $C_A = C_B = 50, 100,$  and  $200$  fF, respectively. The vertical axis is the insertion loss and the reflectivity in dB.



**Figure 23.** The performance of a multi-layer PSS with different switching strategies ( $N=4$ ): the solid line is with binomial switching times; the dashed line is for equal switching times. The vertical axis is the reflectivity in dB.

PSS increases its functionality, although in this case with the added advantage of dynamic reconfiguration. Here, we will again use a transmission-line analog to explore some of the properties of an  $N$ -active-layer PSS. Of interest is the structure's time-averaged reflection coefficient,  $\rho(f)$ . For normal incidence, this can be expressed as

$$\rho(f) = -\left(a_0 + a_1 e^{j2\beta_0 d} + a_2 e^{j4\beta_0 d} + \dots + a_{N-1} e^{j2(N-1)\beta_0 d}\right). \quad (25)$$

This expression is *exact* for the ideal PSS (i.e., active-layer conductances switched repetitively between the values of 0 and  $\infty$ ), since no multiple-reflection phenomena occur within the structure. By analogy with Equation (4), the coefficients  $a_n$  are the normalized "on" times,  $\tau_n/T$ , associated with each active layer, and these

are related by  $\sum_{n=0}^{N-1} a_n = 1$ . Hence, by choosing appropriate values

for  $a_n$ , the multi-layer PSS may be configured dynamically to have different reflectivity characteristics. Equation (25) can be simplified if the PSS structure is assumed to be symmetrical, i.e.,  $a_0 = a_{N-1}$ ,  $a_1 = a_{N-2}$ , etc. Then,

$$\rho(f) = -2e^{j(N-1)\phi} \left\{ a_0 \cos[(N-1)\phi] + a_1 \cos[(N-3)\phi] + a_2 \cos[(N-5)\phi] + \dots \right\}, \quad (26)$$

where  $\phi = \beta_0 d/2$ , and the last term in Equation (26) is  $\frac{1}{2}a_{(N-1)/2}$  for  $N$  odd, and  $a_{(N/2)-1} \cos \phi$  for  $N$  even. Equation (26) is a periodic function over the interval  $\pi$ , which corresponds to the frequency range over which the spacing between adjacent active layers in the PSS changes by  $\lambda/2$ .

If, for example,  $a_n = 1/N$  (i.e. equal "on" times),  $\rho(f)$  will exhibit a  $\sin x/x$  form [22], whereas a maximally flat reflectivity response may be obtained by setting  $a_n = 2^{-(N-1)} \frac{(N-1)!}{(N-1-n)!n!}$ .

These are both shown in Figure 23 for  $N = 4$ .

So far, we have shown how the multiple-active-layer PSS may be configured to have "canonical" reflectivity characteristics, with null positions that are determined solely by the number of active layers. In practice, however, it might be more useful to have a means of dynamically changing the positions of the reflectivity nulls, irrespective of the number of active layers. As a simple example, consider a PSS having two active layers and a PEC backplane: this corresponds to the case for  $N=3$ . Assuming a symmetrical structure, then  $a_0 = a_2$ , and since  $a_0 + a_1 + a_2 = 1$ , this means that  $a_0$  and  $a_1$  are related by Equation [26]:

$$a_1 = 1 - 2a_0, \quad 0 \leq a_0 \leq 0.5. \quad (27)$$

This approach may be extended to higher values of  $N$ , e.g., for  $N=4$ ,  $a_0 = a_3$ ,  $a_1 = a_2$ , and

$$a_1 = 0.5 - a_0, \quad 0 \leq a_0 \leq 0.5. \quad (28)$$

Figure 24 shows the application of Equation (27) to define the "on" times for a PSS containing two active layers. When  $a_0 = 0.5$ , the reflectivity response has a single null at the frequency where  $d = \lambda/4$ . As the value of  $a_0$  decreases, however, the null bifurcates to give two nulls that move apart as "mirror-images." Thus, a reflectivity null may be positioned anywhere within the frequency range  $c/8d \leq f \leq 3c/8d$ , where  $c = 3 \times 10^8$  m/s. Interestingly, if  $a_0 = 0$  and Equation (27) is not satisfied, then the reflectivity characteristic only has a single null, which fills in as  $a_1 \rightarrow 0$  or 1. This case is analogous to that shown in Figures 4 and 5. When the PSS has more active layers, then the use of appropriate "on" time relationships, deduced by induction from Equations (27) and (28), result in the formation of multiple "mirror-image" reflectivity nulls, which can also be tuned dynamically over a wide band of frequencies.


## 11. Conclusions

In this necessarily brief review, we have attempted to introduce some basic concepts concerning dynamic RCS control using an active technique based on the phase-switched screen. Although development and exploitation of the PSS is still at an early stage, the theoretical and experimental work we have reported here and elsewhere confirm the viability of the technique, which we believe to have a number of applications in both the civil [39] and defense fields.

## 12. References

1. W. H. Emerson, "Electromagnetic Wave Absorbers and Anechoic Chambers through the Years," *IEEE Transactions on Antennas and Propagation*, **AP-21**, 4, 1973, pp. 484-490.
2. S. S. Swords, *A Technical History of the Beginnings of Radar*, London, Peter Peregrinus, (IEE History of Technology Series, 6), 1986.
3. W. W. Salisbury, "Absorbent Body for Electromagnetic Waves," US Patent No. 2599944, June 10, 1952.
4. G. G. McFarlane, "The Schornsteinfeger Project," CIOS Target No. 1/549 Radar, 1945.
5. E. F. Knott, J. F. Schaeffer, and M. T. Tuley, *Radar Cross-Section, Second Edition*, Norwood, MA, Artech House, 1993.
6. B. A. Munk, *Frequency Selective Surfaces*, New York, Wiley, 2000.
7. A. Taflove and S. C. Hagness, *Computational Electrodynamics: The Finite-Difference Time-Domain Method, Second Edition*, Norwood, MA, Artech House, 2000.
8. K. N. Rozanov, "Ultimate Thickness to Bandwidth Ratio of Radar Absorbers," *IEEE Transactions on Antennas and Propagation*, **AP-48**, 8, 2000, pp. 1230-1234.
9. R. Zhang, A. Barnes, K. L. Ford, B. Chambers, and P. V. Wright, "A New Microwave 'Smart Window' Based on a Poly(3,4-Ethylenedioxythiophene) Composite," *J. Mat. Chem.*, **13**, 2003, pp. 16-20.
10. R. J. Deri and J. P. Spoonhower, "Microwave Photodielectric Effect in AgCl," *Physics Review B*, **25**, 1982, pp. 2821-2827.
11. R. H. Mattson, "Proposed Method for Controlling and Minimising Reflections from a Surface," *IRE Transactions on Electron Devices*, **ED-8**, 1961, pp. 386-389.
12. S. W. Lee and T. T. Fong, "Electromagnetic Wave Scattering from an Active Corrugated Structure," *Journal of Applied Physics*, **43**, 1972, pp. 388-396.
13. W. W. Lam, C. F. Jou, H. Z. Chen, K. S. Stolt, N. C. Luhmann and D. B. Rutledge, "Millimeter-Wave Diode-Grid Phase Shifters," *IEEE Transactions on Microwave Theory and Techniques*, **MTT-36**, 1988, pp. 902-907.
14. T. K. Chang, R. J. Langley and E. A. Parker, "An Active Square Loop Frequency Selective Surface," *IEEE Microwave and Guided Wave Letters*, **3**, 1993, pp. 387-388.
15. A. Tennant and B. Chambers, "Experimental Phase Modulating Planar Screen," *Electronics Letters*, **34**, 1998, pp. 1143-1144.
16. B. Chambers, "A Smart Radar Absorber," *Smart Mater. Struct.*, **8**, 1999, pp. 64-72.
17. H. Stockman, "Communication by Means of Reflected Power," *Proceedings of the IRE*, **36**, 1948, pp. 1196-1204.
18. R. Bracht, E. K. Miller, and T. Kuckertz, "An Impedance-Modulated-Reflector System," *IEEE Potentials*, **18**, 1999, pp. 29-33.
19. J. Thornton and D. J. Edwards, "Modulating Retro-Reflector as a Passive Radar Transponder," *Electronics Letters*, **34**, 1998, pp. 1880-1881.
20. J. Van Bladel and D. de Zutter, "Reflections from Linearly Vibrating Objects: Plane Mirror at Normal Incidence," *IEEE Transactions on Antennas and Propagation*, **AP-29**, 1981, pp. 629-637.
21. F. Harfoush, A. Taflove, and G. A. Kriegsmann, "A Numerical Technique for Analysing Electromagnetic Wave Scattering from Moving Surfaces in One and Two Dimensions," *IEEE Transactions on Antennas and Propagation*, **AP-37**, 1989, pp. 55-63.
22. A. Tennant, "Reflection Properties of a Phase Modulating Planar Screen," *Electronics Letters*, **33**, 1997, pp. 1768-1769.
23. B. Chambers and A. Tennant, "General Analysis of the Phase-Switched Screen. Part 1: The Single Layer Case," *IEE Proc. - Radar Sonar Navig.*, 2002, pp. 243-247.
24. P. N. Kaleeba, A. Tennant, and J. P. Ide, "Characteristics of Phase-Switched Screens at Oblique Incidence," *Proceedings of the AMTA Symposium*, Boulder USA, 2001, pp. 177-182.
25. H. V. Shurmer, *Microwave Semiconductor Devices*, Pitman, 1970.
26. B. Chambers, "Characteristics of Modulated Planar Radar Absorbers," *Electronics Letters*, **33**, 1997, pp. 2073-2074.
27. B. Chambers and A. Tennant, "Influence of Switching-Waveform Characteristics on the Performance of a Single-Layer Phase-Switched Screen," *IEEE Transactions on Electromagnetic Compatibility*, **EMC-44**, 2002, pp. 434-441.
28. E. J. Watson, "Primitive Polynomials (Mod 2)," *J. Math. Comput.*, **16**, 1962, pp. 368-369.
29. A. Tennant and B. Chambers, "A Single-Layer Tunable Microwave Absorber Using an Active FSS," *IEEE Microwave and Wireless Components Letters*, **14**, 2004, pp. 46-47.
30. A. Tennant and B. Chambers, "An Experimental Dual-Polarised Phase Switched Screen," *Electronics Letters*, **39**, 2003, pp. 119-121.

31. A. Tennant and B. Chambers, "Cylindrical Phase-Switched Screens," *Proceedings of RADAR 2002*, Edinburgh UK, 2002, pp. 123-127.
32. A. Tennant and B. Chambers, "Bi-Static Scattering from Cylindrical Phase-Switched Screens," *Electronics Letters*, **37**, 2001, pp. 1507-1509.
33. B. Chambers and A. Tennant, "The Characteristics of a Salisbury Screen Radar Absorber Covered by a Dielectric Skin," *Electronics Letters*, **30**, 1994, pp. 1797-1799 and **31**, 1995, p. 77.
34. B. Chambers and A. Tennant, "A New Single Layer Phase-Switched Screen Using Double Diode Switching Elements," *Electronics Letters*, **39**, 2003, pp. 1150-1152.
35. M. Cohn, J. E. Degenford, and B. A. Newman, "Harmonic Mixing with an Anti-Parallel Diode Pair," *IEEE Transactions on Microwave Theory and Techniques*, **MTT-23**, 1975, pp. 667-673.
36. A. Tennant and B. Chambers, "Controlled Scattering from PEC Surfaces Using PSS Boundary," *Electronics Letters*, **38**, 2002, pp. 780-781.
37. B. Chambers and A. Tennant, "Progress in Smart Radar Absorbers," *Proc. SPIE*, **4934**, 2003, pp. 190-199.
38. B. Chambers and A. Tennant, "Design and Implementation of a Smart Radar Absorber," IEEE International Symposium on Antennas and Propagation, Columbus OH, USA, 2003.
39. A. Tennant and B. Chambers, "Wind Turbine Generators with Active Doppler Suppression Blades," SPIE Conference on Smart Electronics, MEMS, BioMEMS and Nanotechnology, 2004, San Diego, USA, *Proc SPIE*, **5389**, in press.

**Alan Tennant** received the BEng degree in Electronic Engineering and the PhD degree in Medical Physics, both from the University of Sheffield, UK, in 1985 and 1992, respectively. Between 1985 and 1986, he worked with BAe Systems, Stevenage, UK. In 1992, he joined the Defence and Evaluation Research Agency (DERA), Malvern, UK, where he worked on phased-array antenna systems, before taking up an academic post at the University of Hull, UK. In 2001, Dr. Tennant returned to the University of Sheffield as a Senior Lecturer in the Communications and Radar Group. His research interests include adaptive materials for radar-signature management, novel three-dimensional phased-array antenna topologies, and acoustic array systems. 

IEEE TRANSACTIONS ON ANTENNAS AND PROPAGATION

## Changes of Address

Information regarding subscription addresses is managed by IEEE headquarters. It is *not* maintained, nor can it be changed, by any member of the *Magazine* staff. If you are a member of the IEEE, your subscription is sent to the address in your IEEE member record. Your record can be updated via the Web at <http://www.ieee.org/membership/coa.html>. This can also be done by contacting IEEE headquarters: Member Address Records, IEEE Headquarters, 445 Hoes Lane, Piscataway NJ 08855-1331 USA; Tel: +1 (908) 981-0060 or +1 (800) 678-4333; Fax: +1 (908) 981-9667; E-mail: [address.change@ieee.org](mailto:address.change@ieee.org). If you are an institutional or other non-member subscriber, contact IEEE Customer Service at the above address, telephone, and fax numbers; E-mail: [customer.service@ieee.org](mailto:customer.service@ieee.org). Do *not* send requests to any member of the *Magazine* staff.

## Introducing the Feature Article Authors

**Barry Chambers** received his BEng degree in Electrical Engineering in 1964 and his PhD in 1968, both from the University of Sheffield, UK. In 2002, he received the DEng degree for contributions to the field of active microwave surfaces.

In 1968, he joined the Department of Electrical Engineering at the University of British Columbia, Vancouver, Canada, as a postdoctoral Teaching Fellow, and was appointed Assistant Professor there in 1969. In 1971, he returned to the University of Sheffield, where he is now Professor of Communication Engineering and Head of the Communications and Radar Research Group. His current research interests include evolutionary optimization techniques, synthesis and applications of nano-composite polymer materials with novel electromagnetic properties, electromagnetic wave scattering, low-observable techniques and technology, smart electromagnetic structures, and automated microwave metrology.

Dr. Chambers is a Fellow of the IEE (London) and a Senior Member of the IEEE. He has served on the IEE's Professional Group Committees for Antennas and Propagation and for Radar, Sonar and Navigation. He is currently a member of the IEE's Professional Network Technical Panel for Antennas and Propagation. He has published over 170 scientific journal and conference papers, and has contributed to three books and several patents.

## AP-S Election Results

2005 IEEE Antennas and Propagation Society President

**Richard W. Ziolkowski**

2005 IEEE Antennas and Propagation Society Vice President

**Andrew F. Peterson**

Note: A clerical error led to the omission of two names from the slate for Administrative Committee on the original ballot mailed to AP-S members. As a result, the AdCom vote using that ballot was not valid. A new ballot for the 2005 class of AdCom members has been mailed to the membership. The results of the AdCom election were thus not known as this issue of the *Magazine* went to press. They will be reported in the next issue of the *Magazine*.